2010-01-0148

Development and validation of predictive emissions schemes for quasi-dimensional combustion models

Federico Perini, Enrico Mattarelli, Fabrizio Paltrinieri
University of Modena and Reggio Emilia, Modena, Italy

ABSTRACT

The paper presents the development and validation of phenomenological predictive schemes for quasi-dimensional modeling of pollutant emissions in direct injected Diesel engines. Models for nitric oxide (NO), carbon monoxide (CO), as well as soot and unburned hydrocarbons (HC) have been developed. All of them have been implemented into a DI Diesel engine simulation environment, previously developed by the authors, which features quasi-dimensional modeling of spray injection and evolution, air-fuel mixture formation, as well as auto-ignition and combustion. An extended Zel'dovich mechanism, which takes into account the three main, thermal-NO formation chemical reactions has been developed for predicting NO emissions. A simple, one-reaction soot formation model has been implemented, while a new approach has been proposed for soot oxidation, which considers two different temperature ranges: the well-established Nagle and Strickland-Constable one has been adopted for the highest temperatures, while a new, single-step reaction model has been implemented at the low temperatures. The model for carbon monoxide formation relies on five chemical reactions, whose kinetics are computed exploiting partial equilibrium assumptions, in a system of 11 species. Finally, hydrocarbon emissions have been modeled taking into account the effects of three main sources: fuel injected and mixed beyond the lean combustion limit, fuel yielded by the injector sac volume and nozzle holes, as well as overpenetrated fuel. A detailed comparison with experimental data from a high speed, direct injected diesel engine, carried on for both full and partial load and for a wide range of engine speeds, shows that the models are capable to predict the engine emissions with reasonable reliability.

INTRODUCTION

Since the last years, diesel engine technology is undergoing considerable advances, and research is very active, as modern diesel engines couple high efficiency with constantly increasing environmental friendliness. For their design and optimization, many simulation tools are available as a support of the experimental efforts: among them, the most complete are 3D-CFD software codes coupled with chemical kinetics solvers, which nowadays allow full engine cycle simulation to be run in reasonable amounts of time. Nevertheless, due to the high computational resources required, these tools are more suitable during the design process final stages, where attention is focused on operating and geometric details, while instead simpler, 1D-CFD codes are widely adopted in the early phases, due to their intrinsic capability in modeling the entire engine system and for investigating the interactions among its components. On the other hand, the accuracy of lumped parameters codes is strongly related - especially when dealing with diesel combustion - to a high number of parameters which have to be calibrated on detailed experimental data. In particular, as well known, the combustion process in HSDI engines is strongly dependent on fuel jet atomization and mixing with the surrounding air. For overcoming these problems, a number of quasi-dimensional, multi-zone combustion models has been developed [1-7]. Following this approach, a simplified three-dimensional modeling of the spray zone is applied, introducing a proper number of parcels and radial zones. This approach features, at the same time, a satisfactorily accurate representation of injection, mixing and combustion, while requiring very limited computational resources with respect to full 3D-CFD. Research in the field of quasi-dimensional models is still

focusing on the reduction of calibration parameters, as well as on phenomenological modeling of pollutant emissions, usually based on empirical relations [2,3,14,25,26]. The development of reliable prediction tools for engines operated with alternative fuels, such as blends of diesel and ethanol or other vegetable fuels, as well as gaseous fuels [8-11], is recently gaining interest.

In this paper, the development of four detailed schemes for the prediction of HSDI diesel engines most significant pollutants is presented and discussed, on the bases of well established models, and with some original features devoted to reduce their dependence on tuning parameters. In the following paragraph, the detailed description of the models for nitric oxide, as well as soot, unburned hydrocarbons and carbon monoxide as well as their implementation into the quasi-dimensional diesel engine simulation framework previously developed by the authors [7] is described. The results are then validated and compared to experimental data from a small-bore, high speed, direct injected diesel engine of current production.

QUASI-DIMENSIONAL COMBUSTION MODEL

Before going in depth into the development of the predictive models for pollutant emissions, the quasi-dimensional, multi-zone diesel combustion model previously developed by the authors [7] is introduced. This kind of simplified model – usually called quasi-dimensional, since the three-dimensional representation doesn't involve the whole cylinder, but is limited to the fuel spray jet – is able to predict engine performance with a high degree of accuracy, though requiring limited computational resources. As far as the fuel spray representation is concerned, a pictorial view on how it is generated is shown in Figure 1: finite packages (or 'parcels'), introduced at each computational timestep, represent fuel injected into the cylinder. Each parcel is then subdivided into a fixed number of radial and circumferential zones, which behave autonomously. More in detail, each single parcel in the present model is made up of 35 zones, corresponding to 5 radial and 7 circumferential subdivisions, respectively.

After injection, and exploiting the usual presence of macroscopic charge motion, such as swirl, the spray dynamics are ruled by specific patterns, which are evaluated through empirical relations, while no momentum conservation equation is solved, thus reducing the computational efforts. As far as the evolution of the zones is concerned, specific models are included for computing both physical and chemical processes. First of all, the liquid column breaks up into a fuel spray; after the breakup process, air enters into the zone, and the liquid is atomized into droplets, whose diameter distribution is described in terms of estimated Sauter Mean Diameter. Then, evaporation may occur, being governed by ordinary thermodynamic balances. After ignition delay period for the mixture of air and fuel vapor is completed, combustion starts within the zone. Two types of combustion have been considered: a first premixed phase, where the fuel evaporated during the ignition delay is burnt; and a second diffusive combustion phase, ruled by a different Arrhenius-type kinetic equation. Lastly, the mass of burnt gases within the cylinder due to EGR is modeled as an inert thermal capacity. The detailed description of the multi-zone framework, as well as of relationships and calibration constants can be found in [7]. It is worth to mention that, thanks to some original details introduced in the model (i.e. finite-slab swirl and detailed turbulence modeling, comprehensive of the contributions due to injection and combustion), the model has proved to be reliable across a wide range of engine speeds and loads, and to undergo reduced dependence on calibration constants.

As far as pollutant emissions are concerned, quasi-dimensional models are suitable for the implementation of even detailed schemes, due to the high resolution in modeling the spray zones, whose number can add up to 2000-3000 during the simulation of the power cycle of the engine. Each zone represents indeed a thermo-chemical system, in which equilibria and kinetic reactions occur and are solved. In the following, a detailed discussion of the four models developed for NO, soot, HC and CO estimation is proposed and described.

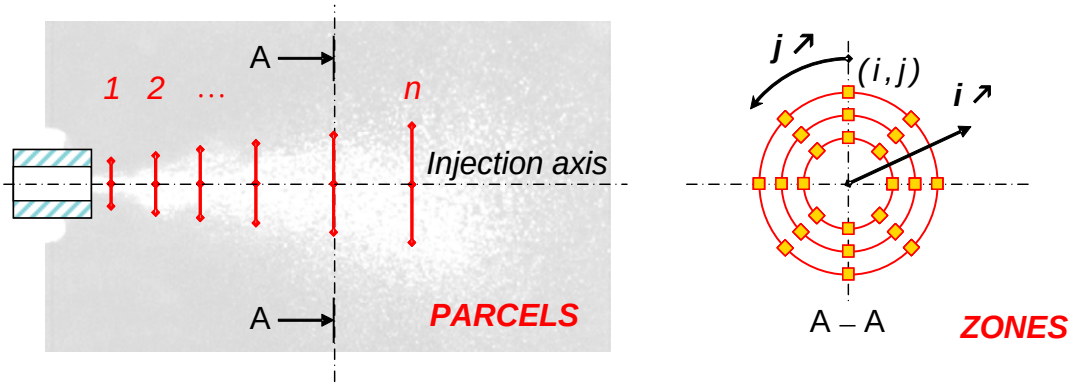

Figure 1 – Subdivision of fuel jet into parcels and zones.

NITRIC OXIDE FORMATION

The minimization of NO_x emissions is one of the most important targets which affect engine design and setup. For this reason, the formation of nitric oxides is under continuous investigation, as many detailed chemical kinetics mechanisms are still under development. It is generally acknowledged [31] that there are three major sources which concur to NO_x formation in combustion systems: the first, usually called thermal-NO, is limited by a high activation energy, and thus is fast enough only at high temperatures; the second mechanism, of prompt or Fenimore NO, takes into account the formation of NO at the flame fronts, deriving from the recombination of the transient CH species. The last source is usually identified in the NO generated from the recombination of nitrous oxide (N_2O), this contribution being significant especially for very lean mixture conditions and low temperatures.

Most detailed diesel combustion kinetic mechanisms include full description of NO formation, where dozens species and reactions are involved [27]. In most phenomenological, multi-zone combustion models, instead, the three-dimensional description of the engine cylinder is simplified, and for this reason simple, equilibrium-based kinetics are usually adopted [2,3,14]. In this work, a similar approach has been followed, even if the NO formation model has been built in an expandable way, so that more complex mechanisms can be fit in the future.

THERMAL NO – The extended Zel'dovich mechanism, made up of three reactions has been considered:

$$\begin{aligned} N_2 + O &\leftrightarrow NO + N \\ N + O_2 &\leftrightarrow NO + O \\ N + OH &\leftrightarrow NO + H \end{aligned} \quad , \qquad (1)$$

where the reaction rate of nitric oxide is expressed as an ODE:

$$\begin{aligned} \frac{d[NO]}{dt} = c_{NO} & k_{f,1}[N_2][O] - k_{b,1}[NO][N] + \\ & + k_{f,2}[N][O_2] - k_{b,2}[NO][O] + \\ & + k_{f,3}[N][OH] - k_{b,3}[NO][H] \end{aligned} \qquad (2)$$

For the sake of reference, the coefficients of the forward reaction rates have been summed up in Table 1. The computation of the NO production rate relies on the knowledge of the concentrations of some other species, such as O, O_2, N, H, and OH. Under the assumption of equilibrium for the dissociation of these species, their concentrations have been estimated by means of a chemical equilibrium program, which details are described more on. As a first attempt of understanding the behavior of the thermal-NO model, when coupled to a quasi-dimensional model, no more reactions have been included other than the Zel'dovich kernel mechanism. In particular, as far as the calibration process is concerned, a unique calibration constant, namely c_{NO}, has been added to the forward reaction rate of the first reaction - see eq. (2). The assumption of modifying the rate limiting reaction has been considered as it is acknowledged that slight discrepancies from the Zel'dovich model can be caused by pressure effects in the equilibrium radical pool [27], and by the assumption that no mixing occurs among the zones [24].

Table 1 – NO kinetics forward reactions rate coefficients in the Arrhenius-type form $k = AT^b \exp(-E/T)$, [31]. Units are cm, mol, s, K.

Reaction	A	b	E
1. N_2+O ↔ NO+N	3.30E12	0.20	0.0
2. N+O_2 ↔ NO+O	6.40E09	1.00	3160.0
3. N+OH ↔ NO+H	3.80E13	0.00	0.0

SOOT FORMATION AND OXIDATION

The term soot is used to indicate the particulates formed during hydrocarbon combustion, when under sub-stoichiometric conditions, for example due to poor air-fuel mixing [22]. Usually, soot emission models are subdivided into two parts: a first one, for computing primary soot particle formation, which takes place in the rich, mostly unburned interior of the diesel spray, and a second one, for estimating its following partial oxidation, occurring in the flame zone, when soot encounters molecular oxygen. Hence, the net soot formation rate is usually computed as the difference between formation and oxidation of soot:

$$\frac{dm_s}{dt} = \frac{dm_{s,f}}{dt} - \frac{dm_{s,o}}{dt}. \quad (3)$$

In this approach, a similar modus operandi has been followed; in particular, focusing on the behavior of the models available in literature for both the phenomena. Usually, [2,3,14,26], both submodels for soot formation and oxidation are tuned by means of two collision frequency values, which act as calibration parameters. In this approach, calibration is limited to the submodel of soot formation only, as the submodel for soot oxidation aims to be reliable at both low and high temperature ranges. In particular, the application of a combination of oxidation models has been addressed, providing satisfactory results, as well as a reduced dependence on model parameters.

FORMATION OF SOOT – Soot formation and growth within an internal combustion engine occurs especially at high temperatures (over 1100K [22]). In most multi-zone, phenomenological combustion models [2,3,14], the soot formation process is represented as a one-way reaction between gaseous fuel and oxygen. This approach,

even if simple, is usually adopted due to the low computational effort required, and because of its empirical nature, which well suits simplified combustion models. Although, in full multidimensional engine simulations, often detailed fuel combustion chemistry is implemented [12], in which a more detailed – but still phenomenological – modeling of soot formation is included. In this paper, a first, one reaction soot formation model by Hiroyasu [3] has been implemented and tuned.

This model features a soot formation rate computed as a first-order reaction of gaseous fuel and oxygen, as follows:

$$\frac{dm_{s,f}}{dt} = A_{s,f}\, m_f\, p^{0.5} \exp\left[-\frac{E_{s,f}}{RT}\right], \qquad (4)$$

where $E_{s,f}$ is the activation energy, R is the universal gas constant, and the collision frequency $A_{s,f}$ acts as a tuning parameter for fitting experimental data. As far as the activation energy is concerned, it is reported in literature to add up to either approximately $E_{s,f}$ = 5.234E4 kJ kmol^{-1} [14,26], or circa $E_{s,f}$ = 8.0E4 kJ kmol^{-1} [9,12]. In this study, the first of the two values has been chosen as reference.

OXIDATION OF SOOT PARTICLES – As far as soot particles oxidation is concerned, only two different approaches can be found in the whole literature about quasi-dimensional combustion models. In particular, most of the combustion models apply a simple, one-way reaction model by Hiroyasu [3], while others exploit the semi-empirical relationship of Nagle and Strickland-Constable (NSC) [15], which relies on the hypothesis of two different oxidation sites: a more reactive one (A), and a less reactive (B), with thermal rearrangement between the sites ruled by an empirical rate constant.

The approach of Hiroyasu is based on modeling of soot oxidation as a second-order reaction between molecular oxygen and soot (considered as gaseous):

$$\frac{dm_{s,o}}{dt} = A_{s,o}\, m_s\, x_{O_2}\, p^{1.8} \exp\left[-\frac{E_{s,o}}{RT}\right], \quad (5)$$

where the collision frequency factor, $A_{s,o}$, acts as a tuning constant for the oxidation model. A direct drawback of this approach is that the model is engine-dependent, since proper calibration has to be made for matching experimental soot measurements.

The behavior of the Nagle and Strickland-Constable model, on the other hand, depends on the partial pressure of oxygen: it is a first order reaction for the lower values, and approaches zero at higher ones. This semi-empirical formulation has proved to be suitable for high-temperature combustion [22]; for this reason, it is widely adopted in predictive engine combustion models. As previously introduced, two types of sites of oxidation are assumed to occur on soot particles [15], ruled by two different surface chemistry rates. Three chemical reactions are assumed to occur:

$$\begin{gathered} A_{site} + O_2 \xrightarrow{k_A} surface\ oxide \xrightarrow{k_A/k_Z} A_{site} + 2CO \\ B_{site} + O_2 \xrightarrow{k_B} B_{site} + 2CO \\ A_{site} \xrightarrow{k_T} B_{site} \end{gathered} \qquad (6)$$

Within this framework, the net soot oxidation rate is given by:

$$\frac{dm_{s,o}}{dt} = \frac{W_c}{\rho_s\, d_s} m_s \left[\left(\frac{k_A p_{O_2}}{1 + k_Z p_{O_2}} \right) x_A + k_B\, p_{O_2} \left(1 - x_A\right) \right] , (7)$$

where W_C = 12 kg/kmol represents the molecular weight of carbon, ρ_s = 2 kg/dm^3 the soot density, and d_s = 1.0E-9 m the soot particle estimated diameter. The proportion between A and B sites is given by the fraction of A sites x_A, which is computed as follows:

$$x_A = \frac{p_{O_2}}{p_{O_2} + k_T / k_B} . \quad (8)$$

As far as the rate constants of the NSC model are concerned, they only depend on the temperature of the mixture within the zone, and are computed as follows [15]:

$$\begin{aligned} k_A &= 20 \cdot \exp[-15100/T] && [g/(cm^2\, s\, atm)] \\ k_B &= 4.46E-3 \cdot \exp[-7640/T] && [g/(cm^2\, s\, atm)] \\ k_T &= 1.51E+5 \cdot \exp[-48800/T] && [g/(cm^2\, s)] \\ k_Z &= 21.3 \cdot \exp[2060/T] && [atm^{-1}] \end{aligned} \quad . \quad (9)$$

A COUPLED OXIDATION APPROACH – Though all the phenomenological models in literature adopt either of the two models for soot oxidation here presented, still these models suffer massive dependence on calibration constants, which usually have to be tuned not only among different engines, but often also when dealing with different loads and rotating speeds. For this reason, a new approach, which couples two different reaction rate models – for high and low temperature ranges - is here presented with the aim of reducing the dependence of the soot oxidation framework on tuning parameters. As it is highlighted by Stanmore et al. [22], the NSC oxidation model is widely adopted within engine simulation codes, because it has been developed analyzing high temperature combustion (> 1700K). Nevertheless, as it has been pointed out by Park and Appleton [23], this model suffers some underestimation of the oxidation rate, so tending to loose validity at lower temperatures.

For this reason, a hybrid oxidation model has been developed, which follows the NSC model for temperatures higher than 1700K, and a different, single-reaction oxidation model which has been defined and implemented for the lowest temperatures range. The formulation of the lower temperatures oxidation model (LTO) is an Arrhenius-type reaction equation:

$$\frac{dm_{s,o}}{dt} = A_{s,o}\, m_s \left(p_{O_2}\right)^{\alpha} \exp\left[-\frac{E_{s,o}}{R\,T} \right] . \quad (10)$$

Following the analysis of the soot oxidation models in [22], the value for the low temperature activation energy has been assumed $E_{s,o}$ = 1.70E5 kJ/kmol, while the order of the reaction, expressed as the exponent on the reaction gas partial pressure p_{O2}, has been chosen α=0.8. Similarly to that defined in Hiroyasu's model, a collision frequency $A_{s,o}$ has been maintained; however, due to the different order of the reaction, it couldn't be regarded as a constant anymore, but has been determined for matching the NSC kinetic rate value at the temperature switch.

In particular, the value for the collision frequency $A_{s,o}$ has been calculated imposing equations (7) and (10) to yield the same value at T_{switch}=1700K, being the expression always dependent on the partial pressure of oxygen:

$$A_{s,o} = \frac{C_1\, p_{O_2}^2 + p_{O_2} + 1}{\left(C_2\, p_{O_2}^2 + C_3 p_{O_2} + C_4\right) C_5\, p_{O_2}^{0.8}}, \quad (11)$$

$$\begin{aligned} C_1 &= \left[k_A / k_T + k_Z\right]_{T=T_{switch}} \\ C_2 &= \left[k_Z / k_T\right]_{T=T_{switch}} \\ C_3 &= \left[k_Z / k_B + k_T^{-1}\right]_{T=T_{switch}} \\ C_4 &= \left[1 / k_B\right]_{T=T_{switch}} \\ C_5 &= \left[\exp\left(-E_{s,o} / RT\right) \rho_s\, d_s\right]_{T=T_{switch}} / W_c \end{aligned} \quad (12)$$

The constants C_1, C_2, ... C_5 only depend on the switch temperature which separates the high and the low temperature ranges. In Figure 2, the so computed LTO collision frequency factor, normalized against the soot formation collision frequency $A_{s,f}$, has been plotted versus the molar fraction of oxygen within the zone, at the reference total pressure p = 120 bar. Figure 3, instead, shows the comparison among the considered soot oxidation models: the NSC model nonlinearly behaves on the Arrhenius plane, as the kinetic rate decreases in the high temperatures range; all the other one-reaction models, instead, are represented as a straight line. From the plot, it's clear that the combined approach NSC+LTO guarantees a higher oxidation rate in the low temperatures range than the simple NSC model, and it behaves similarly to most soot oxidation mechanisms, summarized by an averaged trend (cyan line with squares, in Figure 3) by Smith et al. [22].

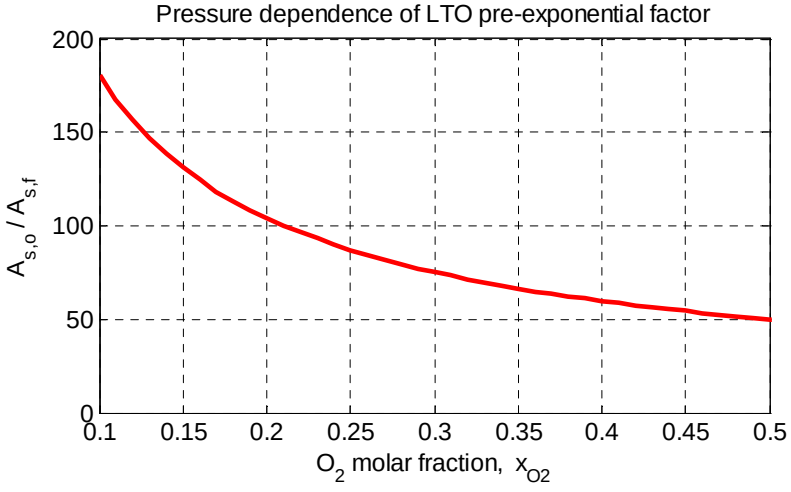

Figure 2 – LTO soot oxidation model collision frequency, normalized with respect to the soot formation collision frequency, vs. oxygen molar fraction, at the reference pressure p = 120 bar.

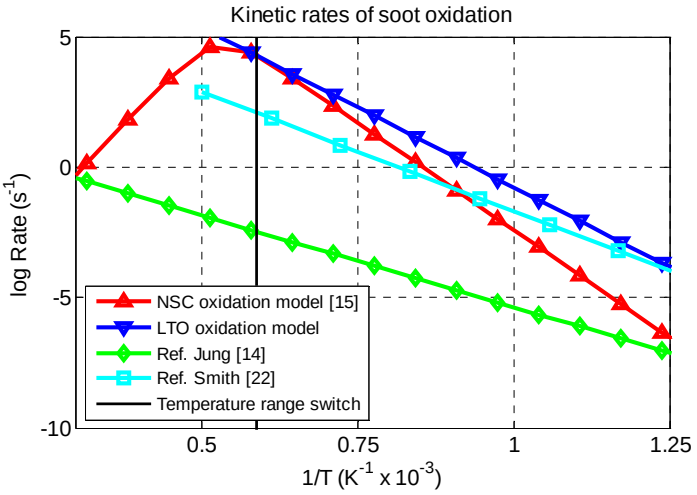

Figure 3 – Arrhenius plot of the kinetic rates of soot gasification in air, following the two oxidation models considered in the soot model, in comparison with literature data, at the reference pressure p = 120 bar.

The green line with diamond marks shows the kinetic law adopted by Jung and Assanis in [14]: it shows similar behavior with the NSC model at the extreme temperature values (>2000K, <800K). About this model, it is worth to remember that the collision frequency has been adopted as a calibration factor for fitting experimental data, and for this reason a slightly uncommon behavior is fully acceptable.

UNBURNED HYDROCARBONS EMISSIONS

The unburned hydrocarbons (HC) being emitted from diesel engines are usually represented in terms of a variety of phenomenological models which capture the different sources causing some amount of fuel not to be burnt during the engine cycle [14,28,29]. Among the others, three main sources of HC have been identified: the first one is the overlean mixture, which is due to the non-uniform spray jet composition during the ignition delay period; the second one is due to fuel released by the injector sac volume, during the expansion stroke, in the form of large drops with very low momentum; the last one is the effect of fuel overpenetration and impingement against the piston bowl and cylinder walls. As far as the effects of crevice volumes on unburned hydrocarbon emissions are concerned, they have been neglected: in spark ignited engines, where flame quenching at the crevice regions, and absorption of homogeneous fuel/air mixture within the oil film layer, play an important role in the overall HC formation. However, in typical DI Diesel engine operation no fuel vapor enters the crevices, as fuel injection, evaporation and combustion usually occur within the piston bowl.

OVERLEANED FUEL – As far as fuel overmixing is concerned, it applies to the fraction of fuel spray injected into the cylinder that, during the ignition delay, mixes below the lean auto-ignition limit. As illustrated in Kuo [29] for alkanes, and extended in [30] to the case of diesel fuel, the lean auto-ignition limit is not appreciably affected by any change in pressure, and the temperature effect on it is even less significant. For this reason, a constant lean flammability limit has been assumed for diesel fuel, and, in accordance with [29] chosen to be Φ = 0.2. For computing the total amount of fuel overmixed during the ignition delay period, it is necessary to estimate the distribution of fuel concentrations across the zones of each parcel. In order to get an appropriate representation of the spray jet distribution a high number of radial and circumferential jet zones would be needed, resulting in a slight increase in total computational time. For this reason, it has been chosen to adopt an analytical relation for describing the radial distribution of the fuel concentration:

$$y(r) = y(0) \cdot \left[1 - \left(\frac{r}{r_{\max}} \right)^{1.5} \right], \quad (13)$$

where the concentration value *y(r)* at a generic distance *r* from the injection axis is modeled following a power law of exponent 1.5 with respect to the normalized radial distance – where the maximum distance, r_{max}, is given by the knowledge of the spray penetration and spray angle [7]. For each parcel, the average fuel concentration can then be estimated as its average over the total number of radial and circumferential zones which define it:

$$\bar{y} = \frac{\sum_{i,j} m_{ev}}{\sum_{i,j} (m_{ev} + m_a)}. \quad (14)$$

The relationship between the average concentration, $\bar{y}$, and the local concentration at the jet centerline, *y(0)*, can be determined via analytical integration as:

$$\bar{y} = \frac{1}{2 r_{\max}} \int_{-r_{\max}}^{r_{\max}} y(0) \cdot \left[1 - \left(\frac{|r|}{r_{\max}} \right)^{1.5} \right] dr. \quad (15)$$

As far as the local radial equivalence ratio is concerned, the following relation is established:

$$\Phi(r) = \left(A/F \right)_{st} \cdot \frac{y(r)}{1 - y(r)}. \quad (16)$$

After some manipulation of equations (13) and (16), an analytical formulation for the radial jet distance farer of which the remaining mixture is beyond the lean auto-ignition limit has been defined:

$$r_L = r_{\max} \cdot \left[1 - \frac{\Phi_L}{y(0) \cdot \left[\left(A/F \right)_{st} + \Phi_L \right]} \right]^{2/3}, \quad (17)$$

and, consequently, the mass fraction of overmixed fuel vapor within the parcel is determined as follows:

$$y_L = \frac{\int_{r_L}^{r_{\max}} y(0) \left[1 - (r/r_{\max})^{1.5} \right] dr}{\int_{0}^{r_{\max}} y(0) \left[1 - (r/r_{\max})^{1.5} \right] dr} = \frac{r_{\max} - r_L - 0.4 \left(r_{\max}^{1.5} - r_L^{2.5} / r_{\max} \right)}{r_{\max} \left(1 - 0.4 \sqrt{r_{\max}} \right)} \quad (18)$$

For the sake of clarity, in Figure 4 the most important aspects of local jet concentration modeling have been pointed out: the radial concentration distribution, the average fuel concentration within the parcel, and the jet area containing overleaned fuel.

As combustion takes place, a fraction of the overlean mixture can burn, thus reducing HC emissions at the end of the power cycle. In order to account for this phenomenon, the well-known Arrhenius-type equation has been

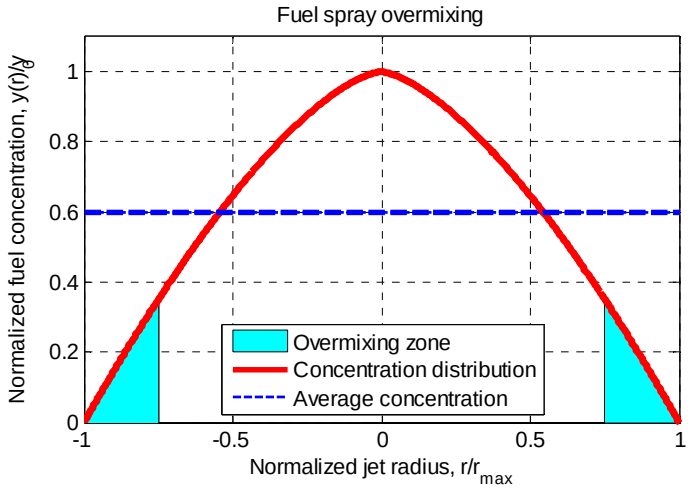

Figure 4 – Normalized fuel concentration versus the normalized jet radius. The blue dotted line shows the average concentration value, while the cyan area refers to the zone occupied by overleaned fuel.

set. Among the empirical correlations available in literature, the one proposed by Jung and Assanis [14] has been chosen:

$$\frac{dm_{HC}}{dt} = -A_{HC}\,\frac{m_{HC}^2}{V}\exp\left(-\frac{E_{HC}}{RT}\right), \qquad (19)$$

being A_{HC} = 1.16E+09 m^3 kg^{-1} s^{-1} the collision frequency factor, and E_{HC} = 7.79E+04 J mol^{-1} the activation energy of HC oxidation.

INJECTOR SAC AND NOZZLE HOLE - The second important source of unburned hydrocarbons consists of the injector nozzle sac volume. As a matter of fact, a non negligible amount of liquid fuel remains into the sac after the end of injection, and then evaporates and mixes late in the expansion stroke, at low velocity and low pressure. As a consequence, it is likely to escape ignition and combustion. In most quasi-dimensional combustion models, which feature HC emissions simulation [14, 32], the empirical relationship by Lakshminarayanan et al. [28] is adopted. In this paper, a similar approach has been implemented, which computes the unburned fuel mass from the injector sac volume as a fraction of the total liquid fuel mass retained by the sac after the end of injection:

$$m_{HC,inj} = y_{sac}\,\rho_l\,V_{sac}, \qquad (20)$$

where the evaporated fuel mass fraction yield from the injector sac, y_{sac}, reported to add up to 0.12 in [14], up to 0.21 in [28], has been found to better match experimental data when being set as y_{sac} = 0.12.

JET OVERPENETRATION – As found by Kuo et al. [29], another important source of HC can be the spray impingement against the cylinder walls and piston bowl. As a matter of fact, though this contribution can be neglected in the case of large bore engines, it plays an important role when dealing with smaller high speed DI

engines, where the jet impingement can cause up to 65% of the total unburned hydrocarbon emissions. In particular, it has been estimated that almost 2% of the fuel mass which has impinged before the start of combustion remains unburned. In order to compute this mass, a lookup table which acts as a pointer for the impinged zones is exploited [7]:

$$m_{HC,imp} = y_{imp} \sum_{i,j \in N_{imp}} m_{i,j} \,, \qquad (21)$$

where N_{imp} represents the set of impinged spray zones mapped into the lookup table, and the unburned overpenetrated fuel fraction has been set y_{imp} = 0.015. In Figure 5, an example of the spray jet zones distribution, projected on a cross section passing through the injection axis, is shown with the aim to clarify the effect of impingement against the piston bowl for a reference engine operating condition.

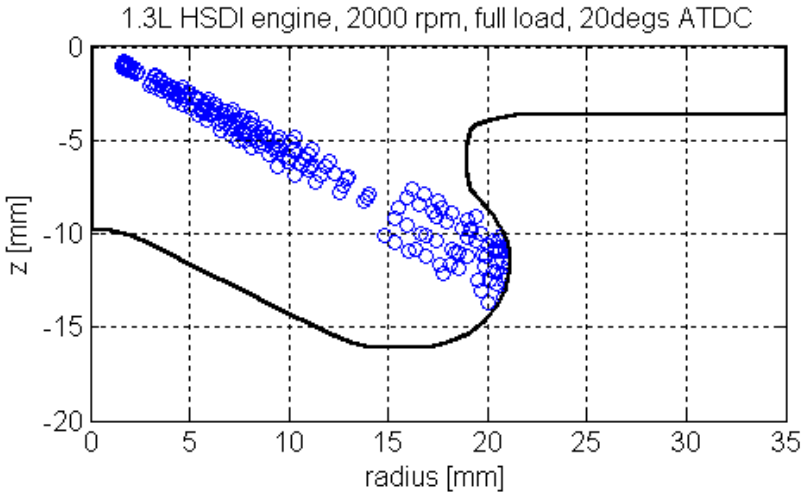

Figure 5 – View of the zones centers (blue circles) projected on the cross section of the chamber sector including the injection axis.

CARBON MONOXIDE

As far as carbon monoxide emissions are concerned, usually, predictive models are implemented within many multi-zone models for the simulation of spark-ignited engines, while instead they are usually omitted in quasi-dimensional models of diesel combustion, due to the relative importance they have in comparison with nitric oxide, soot, and unburned hydrocarbons. However, increasingly restrictive regulations may focus the attention of the diesel engine design process even on carbon oxides. For this reason, a chemical equilibrium-based model for the prediction of CO emissions has been developed and added to the quasi-dimensional diesel combustion framework previously described.

CARBON MONOXIDE FORMATION – As far as carbon monoxide formation is concerned, its kinetics are estimated on the basis of the equilibrium of a system of eleven species and four chemical elements, described in detail in the following paragraph. CO kinetics are then computed evaluating the rates of the reactions which rule CO formation in the post-flame area. In addition to the two reactions proposed by D'Errico et al. [33], a further reaction has been added:

$$\begin{aligned} CO + OH &\leftrightarrow CO_2 + H \\ CO_2 + O &\leftrightarrow CO + O_2 \\ CO + O + M &\leftrightarrow CO_2 + M \end{aligned} \quad , \quad (22)$$

where the reaction rate is expressed as:

$$\frac{d[CO]}{dt} = [R_1 + R_2 + R_3] \cdot \left(1 - \frac{[CO]}{[CO]_{eq}} \right), \qquad (23)$$

$$\begin{aligned} R_1 &= k_{f,1} [CO]_{eq} [OH]_{eq} \\ R_2 &= k_{b,2} [CO]_{eq} [O_2]_{eq} \\ R_3 &= k_{f,3} [CO]_{eq} [O]_{eq} [M]_{eq} \end{aligned} \quad . \quad (24)$$

A detail of the Arrhenius-type forward rate coefficients adopted is presented in Table 2. The reaction rate 1 has been listed three times because, due to strong nonlinearities in the Arrhenius plot, the global reaction rate has been computed as the sum of the three rate coefficients. Lastly, the molecularity *[M]* has been defined as

$$\begin{aligned} [M] = [H_2] + 6.5[H_2O] + 0.4[O_2] + 0.4[N_2] + \\ + 0.75[CO] + 1.5[CO_2]. \end{aligned} \qquad (25)$$

A similar calibration process as that adopted for nitric oxide calculations has been considered: here, the calibration constant c_{CO} premultiplies the three instances of the first reaction, which rules over the mechanism, thanks to the fast recombination of the OH radicals.

Table 2 – CO kinetics forward reactions rate coefficients in the Arrhenius-type form $k = AT^b \exp(-E/T)$ [31]. Units are cm, mol, s, K.

Reaction	**A**	**b**	**E**
1. CO+OH ↔ CO_2+H	1.00E13	0.00	8.05E03
1. CO+OH ↔ CO_2+H	1.01E11	0.00	30.0698
1. CO+OH ↔ CO_2+H	9.03E11	0.00	2.30E03
2. CO_2+O ↔ CO+O_2	2.50E12	0.00	2.41E04
3. CO+O+M ↔ CO_2+M	1.54E15	0.00	1.50E03

CHEMICAL EQUILIBRIUM PROGRAM

The kinetic differential equations, which have to be solved for accurately computing the chemistry of most of the pollutants, often depend on complex chemical systems, made up of many species, and involved in a huge

number of concurrent reactions. Furthermore, the rates of chemical reactions frequently depend on the concentrations of species which aren't directly involved in the reacting system itself, but which unless participate, in steady-state or quasi-steady-state conditions, to the reacting system, thus affecting its behavior.

This is particularly true for internal combustion engines [17], where the chemical system is represented by a gas mixture of variable composition at high temperature and pressure conditions. In such systems, equilibrium conditions are observed for dissociating elements and compounds; for given initial reactants, the degree of dissociation is intensified by the increase in temperature.

In literature [13,18,19], the most widely adopted approach for simulating the equilibrium concentrations in the in-cylinder mixture is obtained considering the main species involved in the stoichiometric combustion of the hydrocarbon fuel, as well as the species arising from the dissociation of elements and compounds. In this analysis, a modified approach based on [13] has been developed. In particular, a total of 12 species has been considered: the fuel – assumed to be a generic hydrocarbon in the form C_nH_m –, plus six species existing in the combustion products (O_2, N_2, H2, CO, CO_2, H_2O), as well as five more species, which are important in internal combustion engines' pollutant formation, which depend on the high-temperature dissociation of the previous ones (O, H, OH, NO, N). As far as the single-component fuel specie is concerned, in this work it has been assumed that it can be well approximated by pure n-dodecane ($C_{12}H_{26}$); this simplifying assumption is vastly adopted not only for quasi-dimensional simulation but also in full 3D multidimensional modelling.

As far as the chemical equilibrium program development is concerned, a general formulation for opposing chemical reactions, which can proceed in both forward and backward directions, has been exploited [16]:

$$\sum_{i=1}^{N} \nu_i' M_i \underset{k_b}{\overset{k_f}{\leftrightarrow}} \sum_{i=1}^{N} \nu_i'' M_i \ , \qquad (26)$$

where M_i denotes the i-th species, N the total number of reacting species, *v'* and *v''* the stoichiometric reaction coefficients of the reactants and of the products, respectively. At thermodynamic equilibrium there is no net change in composition for each of the species, and the equilibrium constant, defined in terms of concentrations as the ratio between the kinetic forward and backward rate constants (k_f, k_b), is defined as:

$$K_c = \frac{k_f}{k_b} = \prod_{j=1}^{N} X_{M_{j,e}}^{\left(\nu_j'' - \nu_j'\right)} , \qquad (27)$$

where the subscript *e* denotes equilibrium conditions, and X_{Mj} the concentration of the j-th species, M_j. Being the species assumed as ideal gases, the equilibrium constant can be written in terms of partial pressures p_p of the species [17]:

$$K_p = \prod_{j=1}^{N} p_{M_{j,e}}^{\left(\nu_j'' - \nu_j'\right)} = \prod_{j=1}^{N} x_{M_{j,e}}^{\left(\nu_j'' - \nu_j'\right)} \cdot p_p^{\left(\nu_j'' - \nu_j'\right)} ; \qquad (28)$$

as, according to Dalton's law, partial pressures are defined as the product of the molar fraction of the species for the total pressure value. In the present work, according to Van't Hoff's equation [16], the equilibrium constant, which depends only on the temperature of the reacting mixture, has been exploited in the form of an explicit dependence on the standard (i.e. at pressure p_0 = 1.0 atm, temperature T_0 = 298 K) Gibbs free-energy change as:

$$\ln\left(K_p\right)=\frac{-\Delta G^o}{R_u T}=\frac{1}{R_u T}\left[\sum_{j=1}^{N}\left(\nu_j''-\nu_j'\right)\Delta g_j^o\right], \quad (29)$$

where the values for the molar standard free energy of formation, Δg^o, are computed from the knowledge of the coefficients for polynomial interpolation [17,20], which depend on the species, and are determined for temperatures ranging the [500K - 1600K] and [1600K - 6000K] ranges:

$$\begin{aligned}\frac{\Delta g_j^o(T)}{R_u T}&=a_{j,1}\left(1-\ln T\right)-a_{j,2}T-a_{j,3}\frac{T^2}{2}+\\&-a_{j,4}\frac{T^3}{3}-a_{j,5}\frac{T^4}{4}-a_{j,6}.\end{aligned} \quad (30)$$

The first estimate of the mole fraction values of the species is computed under the assumption of stoichiometric combustion of the mixture:

$$\begin{aligned}&C_nH_m+O_2+N_2+CO_2+H_2O\rightarrow O_2+N_2+\\&+CO_2+H_2O+H+H_2+N+NO+O+OH+CO,\end{aligned} \quad (31)$$

applying the balances in terms of molar fractions of the species for each of the four atoms present in the system:

$$\begin{aligned}&C)\,n\,x^0_{C_nH_m}+x^0_{CO_2}=\Psi\left[x_{CO_2}+x_{CO}\right]\\&H)\,m\,x^0_{C_nH_m}+2x^0_{H_2O}=\Psi\left[2x_{H_2O}+x_H+2x_{H_2}+x_{OH}\right]\\&O)\,2x^0_{O_2}+2x^0_{CO_2}+x^0_{H_2O}=\Psi\left[2x_{O_2}+2x_{CO_2}+x_{H_2O}+x_{NO}+x_O+x_{OH}+x_{CO}\right]\\&N)\,2x^0_{N_2}=\Psi\left[2x_{N_2}+x_N+x_{NO}\right]\end{aligned} \quad (32)$$

where x denotes molar concentrations, and Ψ the ratio between the total number of moles of the products for each mole of reactants.

The four equations (32) descending from the expression for stoichiometric combustion of the fuel (31) are then coupled with a system of seven dissociation equilibria:

$$\begin{aligned}H_2&\overset{K_{p,1}}{\leftrightarrow}2H\\O_2&\overset{K_{p,2}}{\leftrightarrow}2O\\N_2&\overset{K_{p,3}}{\leftrightarrow}2N\\2H_2O&\overset{K_{p,4}}{\leftrightarrow}2H_2+O_2\\H_2O&\overset{K_{p,5}}{\leftrightarrow}OH+\tfrac{1}{2}H_2\\H_2+CO_2&\overset{K_{p,6}}{\leftrightarrow}H_2O+CO\\H_2O+\tfrac{1}{2}N_2&\overset{K_{p,7}}{\leftrightarrow}H_2+NO\end{aligned} \quad (33)$$

According to (28,29), the equilibrium constants, $K_{p,j}$, for each of the equilibria, are known as a function of temperature and pressure, and the only unknown quantities are the molar concentrations of the species. In this way, a non-linear system of dimension 11 x 11 is derived. For the solution procedure, the Newton-Raphson method has been chosen, with initial values for the molar concentrations guessed from the computation of the stoichiometric combustion equation. For the sake of clarity, in Figure 6 the trends in terms of concentrations of the species which take the most important roles in pollutant formation are plotted, at an arbitrary 100 bar mixture pressure value, and two different equivalence ratios, $\Phi = 0.5$ (lean) and $\Phi = 2.5$ (rich), respectively.

Since exhaust gas recirculation is of crucial importance in modern engines, the chemical equilibrium program has been given the possibility of taking into account non-zero EGR mass fractions affecting the composition of the unburned in-cylinder mixture. For this purpose, a simplified approach has been followed for defining a set of parameters to be optimized. First of all, the EGR ratio has been calculated as a molar fraction of intake air from:

$$x_{EGR} = \frac{n_{EGR}}{n_{EGR} + n_a}, \qquad (34)$$

where n_a represents the number of moles of fresh charge within the cylinder, while n_{EGR} indicates the total EGR moles, computed as:

$$n_{EGR} = \sum_{\lambda \in N_s} n_\lambda . \quad (35)$$

The N_s EGR species set has been defined a priori, and includes the 11 species considered in the equilibrium program, whose concentrations have been gathered from the chemical composition of a sample exhaust gas mixture, derived from 3D-CFD calculations carried on with a detailed chemistry combustion model [21]:

$$N_s = \{O_2, N_2, CO_2, H_2O, H, H_2, N, NO, O, OH, CO\} \qquad (36)$$

For the sake of reference, the detailed composition, in terms of molar fractions, of the sample EGR mixture has been summed up in Table 3. In Figure 7 the influence of EGR fraction on burned gas composition, for a stoichiometric air-fuel mixture, is highlighted by comparing a no-EGR case to a 50% EGR fraction, at the same 100 bar reference pressure value. Although mitigated by the semi-logarithmic plot type, which is necessary due to the wide range of molar fractions, significant differences can be noticed among the molar fractions of the species for the two different cases.

Table 3 – Molar fraction composition of the species in the EGR mixture here considered.

O_2	**N_2**	**CO_2**	**H_2O**	**H**	**H_2**
9.9e-2	7.5e-1	7.2e-2	7.5e-2	3.5e-5	1.2e-3
N	**NO**	**O**	**OH**	**CO**	
2.5e-11	5.7e-5	1.9e-5	1.1e-4	4.1e-3	

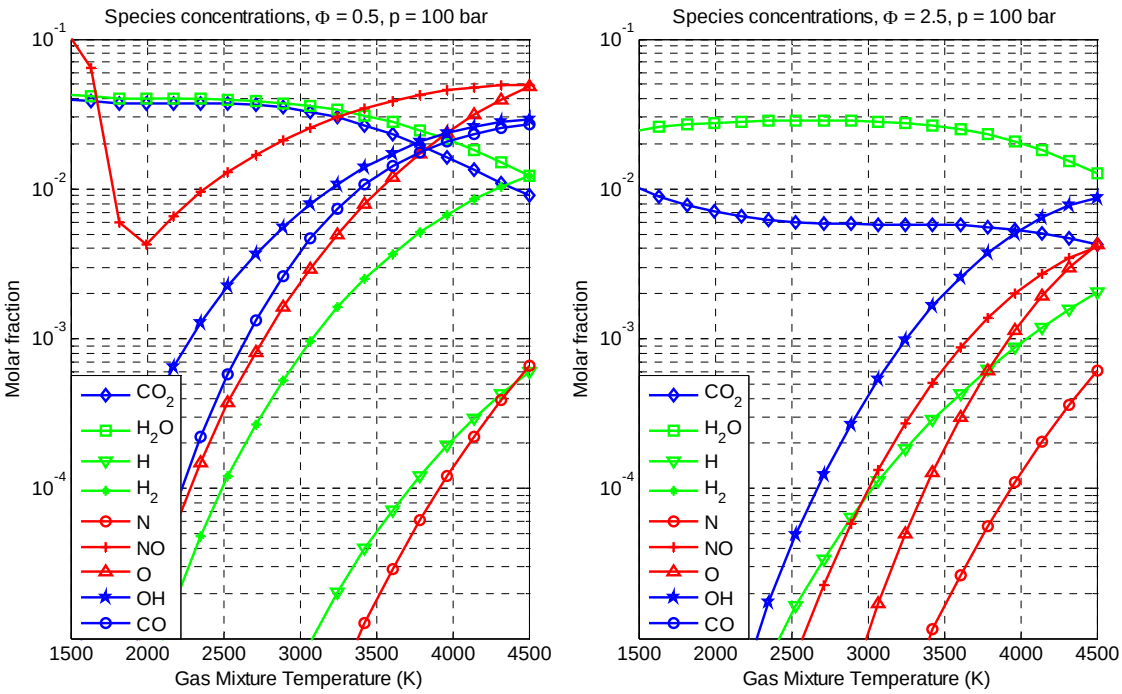

Figure 6 - Species concentrations computed by the chemical equilibrium program, for two different mixture equivalence ratios, at 100 bar pressure.

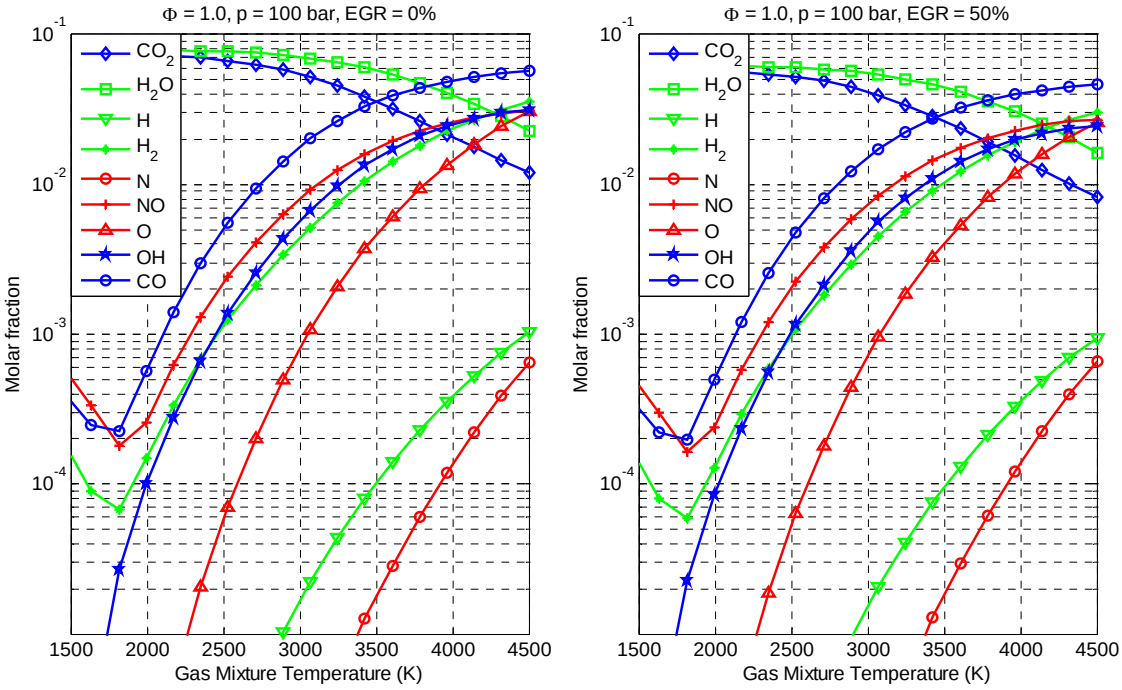

Figure 7 - Species concentrations computed by the chemical equilibrium program, stoichiometric equivalence ratio, and different EGR fractions.

SPARSE INDEXING SOLUTION – The framework for computing equilibrium conditions of the reacting air-fuel mixture has been implemented in Matlab ®, using a modular and flexible architecture. The huge number of parcels and zones which characterizes quasi-dimensional models [7] can make the calculation of chemical equilibria computationally very demanding: considering a simulation time-step of 1°CA, and 2000 zones within the cylinder, a total of about 200.000 chemical equilibria have to be computed during the whole simulation.

For this reason, a fast computation scheme has been developed and implemented into the equilibrium program with the aim of reducing the computational efforts. The Newton-Raphson algorithm for solving the nonlinear system of 11 equilibria acts by substituting a unique nonlinear system of equations with the solution of many linear systems. These systems are so characterized by small, dense coefficient matrices, which have to be solved many times for reaching convergence:

$$J_F\left(\bar{x}_n\right)\left(\bar{x}_{n+1}-\bar{x}_n\right)=-\bar{F}\left(\bar{x}_n\right), \quad (37)$$

where the array $\bar{x}$ contains the eleven unknown species, $\bar{F}$ is the array representation of the eleven equations, and J_F its 11-by-11 Jacobian matrix; the subscript n indicates the current iteration step.

Computing a huge number of independent systems requires Matlab to allocate and deallocate small memory regions many times, thus dramatically increasing the total computational time. For this reason, a vectorized approach has been coded, for substituting the solution of many very small linear systems with few, large-dimension ones. In this approach, a unique equilibrium computation is launched at each timestep, covering all the zones within the cylinder: the many elementary linear systems are concatenated into a unique system of bigger size. First of all, the Jacobian matrices for each of the spray zones are collapsed into a unique block diagonal matrix of the type:

$$\bar{J}_F\left(\bar{x}_n\right)=\begin{bmatrix} \bar{J}_{F,1}\left(\bar{x}_{n,1}\right) & 0 & \cdots & 0 \\ 0 & \bar{J}_{F,2}\left(\bar{x}_{n,2}\right) & \cdots & 0 \\ \vdots & \vdots & \ddots & \vdots \\ 0 & 0 & \cdots & \bar{J}_{F,nz}\left(\bar{x}_{n,nz}\right) \end{bmatrix}, \quad (38)$$

where the subscripts 1,2,…,n_z indicate the spray zones, and n the iterative step; while the array of the unknown concentrations and of the function are concatenated into two unique arrays:

$$\begin{aligned} \bar{x}_n &= \begin{bmatrix} \bar{x}_{n,1}^T & \bar{x}_{n,2}^T & \cdots & \bar{x}_{n,nz}^T \end{bmatrix}^T \\ \bar{F}\left(\bar{x}_n\right) &= \begin{bmatrix} \bar{F}^T\left(\bar{x}_{n,1}\right) & \bar{F}^T\left(\bar{x}_{n,2}\right) & \cdots & \bar{F}^T\left(\bar{x}_{n,nz}\right) \end{bmatrix}^T \end{aligned} \quad (39)$$

The global Jacobian, J_F, which size can add up to 2.0E5, is then stored in sparse indexing format. Lastly, as solution procedure, a conjugate gradient sparse solver method has been exploited. Following this procedure, benchmarks on an AMD Turion X2-64 powered laptop have shown that the new vectorized solution procedure allows a dropdown in computational time needed by the equilibrium program, during a complete quasi-dimensional engine simulation, by circa 97%.

RESULTS AND DISCUSSION

The models of pollutant emissions implemented in the multi-zone diesel combustion framework previously developed [7] have then been validated on a current production small-bore, high speed, direct injected Diesel

engine, whose main parameters are summed up in Table 4. The engine is turbocharged and after-cooled, and features a common-rail injection system working at 160 MPa maximum pressure. Injection strategy features a unique pulse at full load and at high engine revs, while multiple pulses are adopted at the lowest revs and at partial loads: one or two pre/pilot injections are injected before the main pulse. For the sake of reference, the full validation of the fuel injection, spray dynamics and combustion can be found in [7]. For each of the pollutants, a total of 7 engine operating conditions has been spanned: four different rotating speeds at full load, ranging from 1500rpm to 4000rpm, and three more engine revs at 50% load: 1500, 2000 and 3000rpm, respectively.

Table 4 – Main engine specifications.

	1.3L HSDI
Engine type	4-S Diesel
Number of cylinders	4
Total displacement [cm^3]	1248
Bore [mm]	69.6
Stroke [mm]	82
Compression ratio	17.6:1
Valves per cylinder	4
Injection system	common-rail
Max injection pressure [MPa]	160
Injector hole diameter [mm]	0.121
Number of injector holes	6

NITRIC OXIDE – The calibration of the model for nitric oxide formation has been carried out by adding a calibration constant c_{NO} = 1.28 to the forward reaction coefficient of the first reaction in the model, at the reference case of 2000rpm, full-load. In Figure 8, the results of the simulations have been plotted in comparison with the experimental data, measured at the exhaust port: the Zel'dovich model, which is acknowledged to own up to 50% error in NO estimation [27], shows indeed very accurate data, especially at full load, where the global error never exceeds the 36% value obtained at 1500 rpm. Slightly greater error values have instead been observed at partial load, where the simple, thermal-NO model exceeds in NO prediction up to 67% at 3000 rpm. Unless the worst performance of the NO formation model at partial load, it is worth to notice that no change in the tuning constant has been applied. Future improvements to the model may include the implementation of a pressure-dependence trend of the rate constants, in order to better suite the changes in engine load, in presence of higher global equivalence ratios, as well as the adoption of an extended Zel'dovich mechanism, for taking into account the effects in NO formation due to prompt NO and NO generated via nitrous oxide [31].

SOOT – Calibration of the soot model has been carried out at the 2000 rpm, full load, reference operating condition. Figure 9 shows the comparison, in terms of instantaneous in-cylinder soot mass, among five different values of the calibration parameter, $A_{s,f}$. Then, a further analysis has been carried on to understand how significantly different would the model behave if considering soot particle sizes lower than the typical primary particle size of about 25-30 nm [22]. In particular, a higher particle size would lead to transient soot oxidation even slightly far during the expansion stroke; on the other hand, a smaller particle dimension would cause a very limited soot formation peak. For these reason, the typical size $d_s = 30\ nm$ has been chosen. The overall results provided by the soot formation and oxidation submodels implemented are plotted in Figure 10, at both full and partial loads. The histograms show very good accordance between the simulated and the experimental data. As acknowledged in literature [3,14], even simple modeling of the very complex soot formation process is able to predict its emissions with reasonable accuracy, the only drawback being the need to calibrate the model constants when changing engine revs and load. The adoption of a new oxidation model which is able to fit both the low and the high temperature ranges allows calibration to be limited to the soot formation pre-exponential factor only, without needing to tune also the soot oxidation pre-exponential factor, as usually occurs in literature adopting Hiroyasu's model [2,3,14,26]. In the present work, the calibration constant has been maintained unvaried for the whole revving range, and only changed as a function of load: the value $A_{s,f} = 100\ s^{-1}\ atm^{-0.5}$, valid at full load, has been halved to $A_{s,f} = 50\ s^{-1}\ atm^{-0.5}$ at 50% load. As shown in Figure 10, it is possible to state that the adopted model is able to capture the experimental measurements in terms of both absolute values and trends with respect to engine revs.

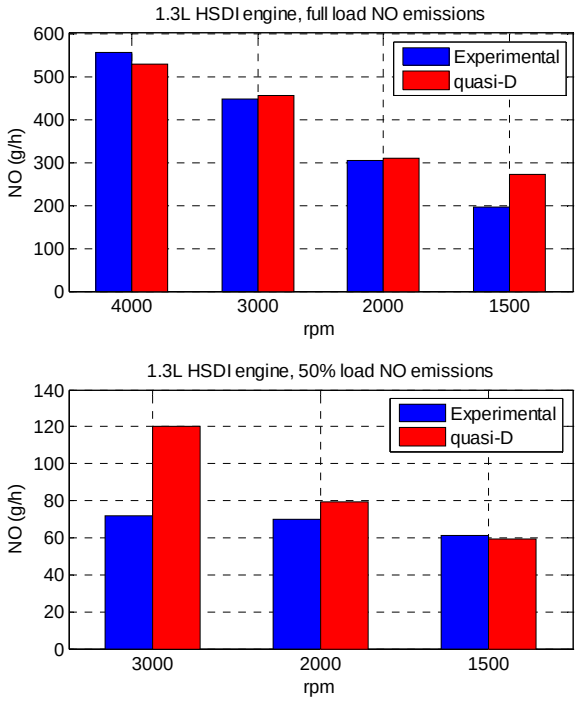

Figure 8 – Comparison between experimental and simulated global engine NO emissions.

UNBURNED HYDROCARBONS – As far as unburned hydrocarbon emissions are concerned, the results have been plotted in Figure 11, comparing the simulated contributions to the total amount of HC, due to overleaned mixture, injector nozzle volume, and overpenetrated fuel, to overall experimental data. The results of the simulations, where no tuning parameters have been changed across the different engine revs and loads, show pretty fair agreement with the experimental measurements at all the regimes and loads computed, even if the

model suffers some overestimation of the HC production at the lowest rpm values, particularly for partial load conditions.

As already acknowledged in [28], the contribution to the total HC emissions due to overleaned fuel is much more significant at the lowest loads. Furthermore, the contribution of overpenetrated fuel is significant at low

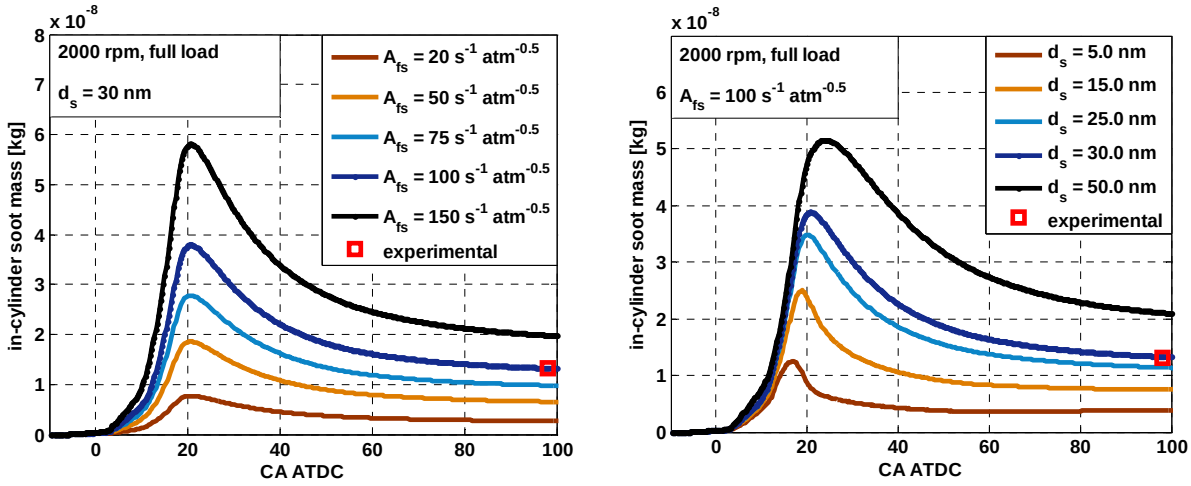

Figure 9 - Calibration of soot emissions model, at 2000 rpm, full load. Left: influence of the soot formation preexponential factor onto the in-cylinder soot mass during the power cycle. Right: Analysis of different soot particle sizes, at the chosen $A_{s,f}$ value.

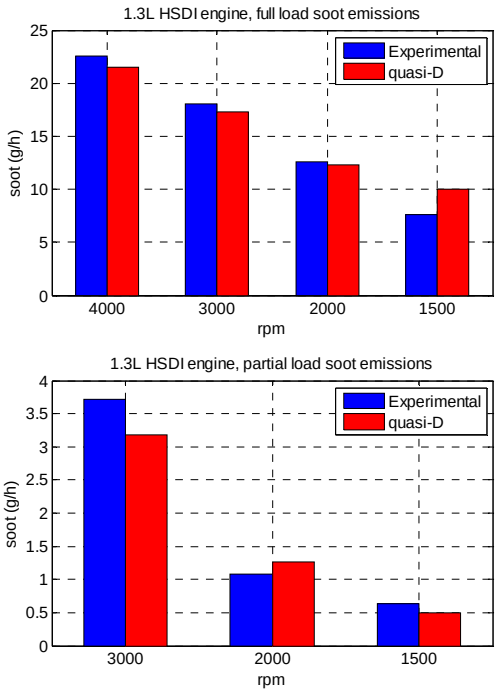

Figure 10 – Comparison between experimental and simulated engine soot emissions, with Hiroyasu's formation model and NSC+LTO soot oxidation model.

engine rpms and partial loads. This is in agreement with literature [28,29], where this source of HC is recognized to play an important role, especially in small-bore diesel engines. Lastly, the injector nozzle volume accounts for a considerable amount of HC especially at full loads, where the other effects are almost negligible.

CARBON MONOXIDE – Similarly to the model which accounts for NO formation, also the simulations of carbon monoxide are calibrated by means of a calibration constant which corrects the forward rate coefficient of the first reaction listed in Table 2. A unique tuning parameter $c_{CO} = 38.5$ has been applied to all the simulations, whose results have been plotted in Figure 12. It is interesting to notice that the behavior of the model shows many similarities, if compared to the model of NO emissions. First of all, it is able to predict the global CO engine emissions with a high degree of accuracy, especially at full load, where the discrepancy between the computed value and the experimental datum is always smaller than 32%, this latest value occurring at 1500 rpm, where also the NO model showed the worse agreement. Slightly worse data can instead be observed at 50% load: still, the datum at 1500rpm shows the highest relative error. Anyway, the computed emissions values, across the three engine rotational speeds simulated, show acceptable match in comparison with experimental data, since the relative error is always less than 63%.

IN-CYLINDER SPATIAL DISTRIBUTIONS – Among the capabilities of the multi-zone approach, some considerations about the spatial distribution of pollutants can be made. In particular, in Figure 13, the concentrations of nitric oxide, carbon monoxide and soot have been plotted, at the calibration reference operating condition (2000 rpm, full load). A total of 9 relevant crank angle values have been chosen, allowing to analyze the behavior of the model at both the pilot injection and the main pulse. From the images, it is possible to observe the consistent and reliable behavior of the model at each of the pollutants. As a drawback, some non-homogeneous appearances observed in the images depend on the quasi-dimensional formulation adopted in this work, which doesn't feature any mass or energy exchange between each zone and the surrounding ones. This latest drawback may be the source for some slight deviation in the results from the experimental measurements, especially occurring at the kinetically-driven NO and CO models, at partial load.

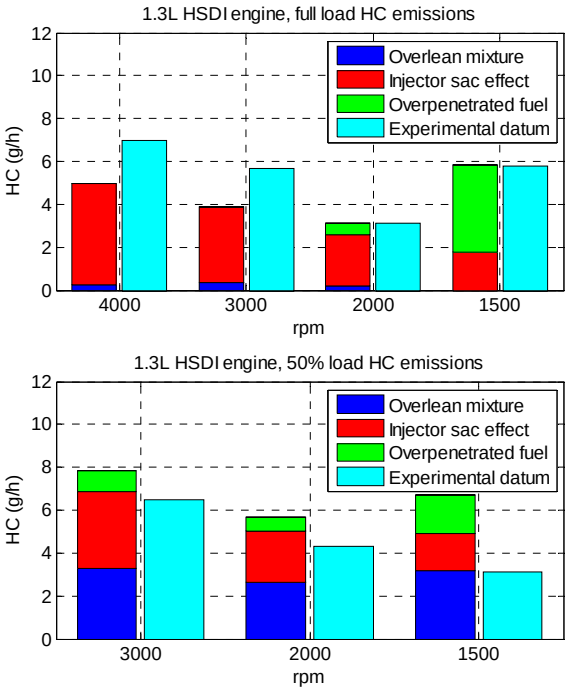

Figure 11 – Comparison between experimental and simulated global engine unburned hydrocarbons emissions.

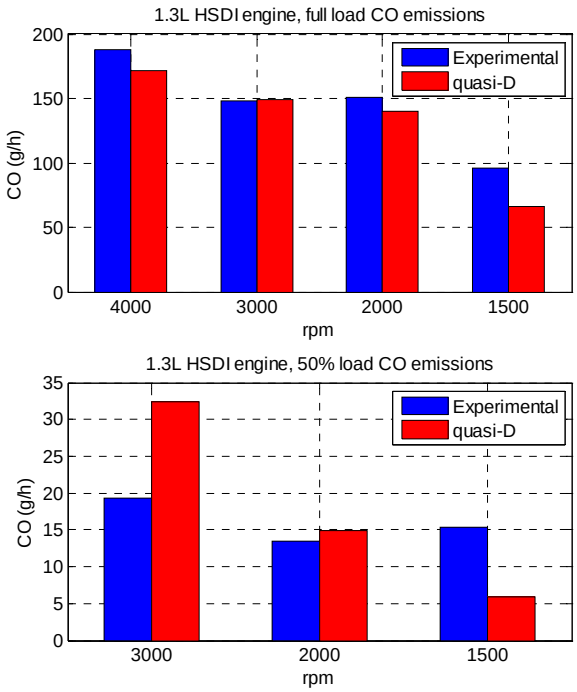

Figure 12 – Comparison between experimental and simulated overall engine CO emissions.

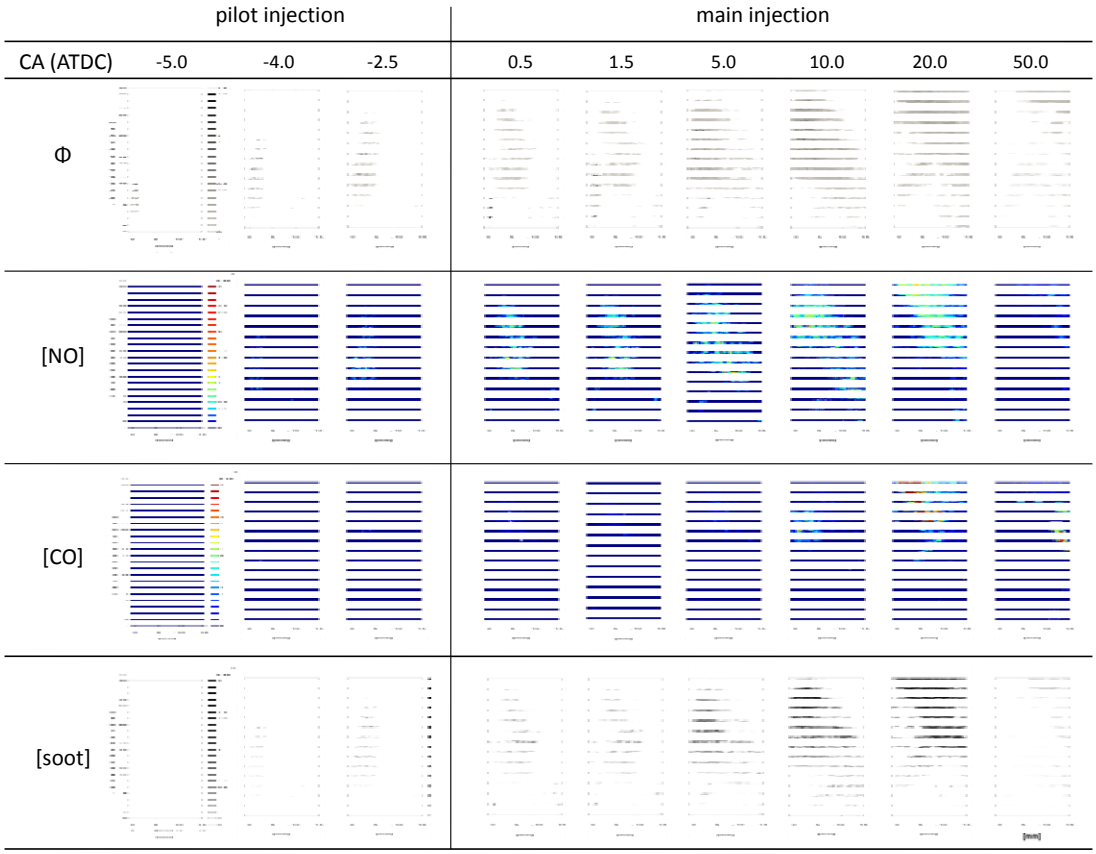

Figure 13 - spatial distribution of in-cylinder equivalence ratio, NO, CO and soot, at 2000 rpm, full load. Concentrations of NO and CO are [kmol m^{-3}], soot number density is in particles per volume unit [m^{-3}].

CONCLUDING REMARKS

Four phenomenological models of pollutant emissions from high speed, direct injected diesel engines have been developed and implemented into a quasi-dimensional, multi-zone engine simulation environment previously developed by the authors. The models for the prediction of NO and CO rely on a chemical equilibrium program which computes the dissociation equilibria of the eleven species considered. On the basis of some partial equilibrium assumptions, two simple reaction mechanisms of three and five reactions, respectively, have been exploited. As far as unburned hydrocarbons are concerned, three main sources have been considered: leaned out fuel during the ignition delay period - and partially oxidized as combustion occurs -, fuel retained by the injector sac and nozzle volume - and released late in the expansion stroke -, and spray impingement against the cylinder walls and piston bowl. Soot formation has been modeled through a simple, well-established, Arrhenius-type reaction, calibrated at full and partial load with a tuning constant. As far as soot oxidation is concerned, a new, coupled approach has been presented which combines the well known NSC oxidation mechanism in the high temperature range, and a one-reaction mechanism (LTO, low temperature soot oxidation), which constants have been retrieved from literature, for well suiting the range of temperatures below 1700K.

A full validation of the proposed models has been presented against a set of experimental data from a small-bore, current production, HSDI diesel engine, over a wide range of engine speeds, at both full and partial (50%) load. The results of the simulations showed that the models are able to predict not only trends, but also point-to-point values of pollutant emissions with a reasonable accuracy, and with a smooth behavior across the whole range of speeds and loads. More in detail, some conclusions can be drawn:

- The Zel'dovich model is able to predict NO emissions with reasonable accuracy, even if it is affected by non negligible error especially at low engine speeds and partial loads. The analysis of the spatial distribution of NO concentrations shows that a possible candidate for this inaccuracy may be the absence of mass and energy exchanges among the fuel jet zones. This aspect needs to be further investigated in the future; furthermore, in order to reduce the kinetic model dependence on pressure and load, a future implementation of an extended model, accounting for more detailed mechanisms is desirable;
- Though the models for soot formation and oxidation are simple, they are able to predict soot emissions with a high degree of accuracy; the only drawback is the need for adopting two different formation tuning constants at full and partial load. As the new oxidation model proposed doesn't need to change calibration parameters when dealing with different engine loads, it should be worth implementing a more detailed, multi-step phenomenological formation model, which could further reduce the dependence on calibration parameters. A possible candidate is the nine-step phenomenological model by Tao et al. [12];
- The model for unburned hydrocarbon emissions has been acknowledged to give back satisfactory results in terms of global HC emissions. Furthermore, its behavior well follows small bore engines operation, where it is established that overpenetration is dominant, especially at the lowest speeds, while overleaned mixture accounts for most of HC emissions at partial loads;
- The CO formation model similarly behaves as the Zel'dovich mechanism for NO: at full load, it matches the experimental data with a high degree of precision, while - at partial load - the prediction is less accurate. A possible solution to this drawback could be the introduction of pressure dependence of the rate coefficients, which may improve the predictive ability of the model, especially at different engine loads.

In conclusion, the previously developed diesel engine simulation environment has been enriched by the implementation of reliable, predictive pollutant emissions models, which include nitric oxide, as well as carbon monoxide, unburned hydrocarbons and soot. In the future, the application of the code will be suitable for a range of applications, including, for instance, engine optimization, thanks to its reliability both in terms of

performance and emissions, and thanks to the limited computational times required by a simulation, which can add up to 2 minutes for the engine power cycle.

REFERENCES

1. D.N.Assanis, J.B.Heywood – "Development and Use of a Computer Simulation of the Turbocompounded Diesel System for Engine Performance and Component Heat Transfer Studies", SAE paper 860329, 1986.
2. D. Jung, D.N. Assanis, "Multi-Zone DI Diesel Spray Combustion Model for Cycle Simulation Studies of Engine Performance and Emissions", SAE paper 2001-01-1246.
3. H. Hiroyasu, T. Kadota, M. Arai, "Development and Use of a Spray Combustion Modeling to Predict Diesel Engine Efficiency and Pollutant Emissions (Part 1 Combustion Modeling)", Bull. JSME 26 (1983), 569-575.
4. D.T. Hountalas, D.A. Kouremenos, E.G. Patriotis, V. Schwarz, K.B. Binder, "Using a Phenomenological Multi-Zone Model to Investigate the Effect of Injection Rate Shaping on Performance and Pollutants of a DI Heavy Duty Diesel Engine", SAE paper 2002-01-0074.
5. T.Cerri, A. Onorati, E. Mattarelli, "1D Engine Simulation of a small HSDI Diesel Engine Applying a Predictive Combustion Model", ASME Journal of Engineering for Gas Turbines an Power 130 (2008), 012802, 1-10.
6. P. Zhou, S. Zhou, D. Clelland, "A modified quasi-dimensional multi-zone combustion model for direct injection diesels", International Journal of Engine Research 7 (2006), 335 – 345.
7. F. Perini, E. Mattarelli, "Development and Calibration of a Quasi-Dimensional Combustion Model for HSDI Engines", submitted for publication to International Journal of Engine Research, JER509
8. C.D. Rakopoulos, K.A. Antonopoulos, D.C. Rakopoulos, "Development and application of multi-zone model for combustion and pollutants formation in direct injection diesel engine running with vegetable oil or its bio-diesel", Energy Conversion and Management 48 (2007), 1881–1901.
9. C.D. Rakopoulos, K.A. Antonopoulos, D.C. Rakopoulos, D.T. Hountalas, "Multi-zone modeling of combustion and emissions formation in DI diesel engine operating on ethanol–diesel fuel blends", Energy Conversion and Management 49 (2008), 625-643.
10. C.D. Rakopoulos, K.A. Antonopoulos, D.C. Rakopoulos, "Multi-zone modeling of Diesel engine fuel spray development with vegetable oil, bio-diesel or Diesel fuels", Energy Conversion and Management 47 (2006), 1550-1573.
11. C.D. Rakopoulos, D.C. Rakopoulos, D.T. Hountalas, E.G. Giakoumis, E.C. Andritsakis, "Performance and emissions of bus engine using blends of diesel fuel with bio-diesel of sunflower or cottonseed oils derived from Greek feedstock", Fuel 87 (2008), 147–157.
12. F. Tao, R.D. Reitz, D.E. Foster, Y. Liu, "Nine-step phenomenological diesel soot model validated over a wide range of engine conditions", International Journal of Thermal Sciences 48 (2009), 1223–1234.
13. C.D. Rakopoulos, D.T. Hountalas, E.I. Tzanos, G.N. Taklis, "A fast algorithm for calculating the composition of diesel combustion products using 11 species chemical equilibrium scheme", Advances in Engineering Software 19 (1994), 109-119.
14. D. Jung, D.N. Assanis, "Quasidimensional Modeling of Direct Injection Diesel Engine Nitric Oxide, Soot, and Unburned Hydrocarbon Emissions", Journal of Engineering for Gas Turbines and Power 128 (2006), 388-396.
15. J. Nagle, R.F. Strickland-Constable, "Oxidation of carbon between 1000-2000°C", Proceedings of the fifth conference on carbon – London, Pergamon Press (1962), p.154 – 164.
16. K. K. Kuo, Principles of Combustion. John Wiley and Sons, 1986. ISBN 0-471-09852-3.
17. R.S. Benson, Advanced Engineering Thermodynamics. Pergamon Press, 1967.

18. D.N.Assanis, J.E. Ekchian, R.M.Frank, J.B. Heywood – “A Computer Simulation of the Turbocharged Turbocompounded Diesel Engine System: a Description of the Thermodynamic and Heat Transfer Models”, NASA Technical Report, NASA-CR-174971, 1985.
19. R.A. Svehla, B.J. McBride, “Fortran IV Computer Program Calculations of Thermodynamic and Transport Properties of Complex Chemical Systems”, NASA TN D-7056, 1973.
20. R.S. Benson, N.D. Whitehouse, “Internal Combustion Engines”, Pergamon Press, 1979.
21. L. Montorsi, C.A. Rinaldini, V.I. Golovitchev, “CFD Combustion and Emission Formation Modeling for a HSDI Diesel Engine Using Detailed Chemistry”, Paper ICE2006-1506, Proceedings of the ASME Fall technical Conference, November 5-8, 2006.
22. B.R. Stanmore, J.F. Brilhac, P. Gilot, “The oxidation of soot: a review of experiments, mechanisms and models”, Carbon 39 (2001), 2247 – 2268.
23. C. Park, J.P. Appleton, "Shock-tube Measurements of soot oxidation rates", Combustion and Flame 20 (1973), 369-379.
24. R.R. Raine, C.R. Stone, J. Gould, "Modeling of Nitric Oxide Formation in Spark Ignition Engines with a Multizone Burned Gas", Combustion and Flame 102 (1995), 241-255.
25. T. Cerri, "Multi-zone Combustion Models for predicting performance and pollutant emissions from SI and Diesel engines", PhD Thesis, Politecnico di Milano, 2002.
26. G. Wang, G.X. Li, T. Liu, L. Chen, X. Zhang, J. Lu, "A Developed Model for Emissions Prediction of a DI Diesel Engine", SAE paper 1999-01-0233, 1999.
27. R. Miller, G. Davis, G. Lavoie, C. Newman, T. Gardner, "A Super-Extended Zel'dovich Mechanism for NOx Modeling and Engine Calibration", SAE paper 980781, 1998.
28. P.A. Lakshminarayanan, N. Nayak, S.V. Dingare, A.D. Dani, "Predicting Hydrocarbon Emissions From Direct Injection Diesel Engines", ASME Journal of Engineering for Gas Turbines and Power 124 (2002), 708-716.
29. T.W. Kuo, K.J. Wu, S. Henningsen, "Effects of Fuel Overpenetration and Overmixing During Ignition Delay Period on Hydrocarbon Emissions From a Small Open-Chamber Diesel Engine", ASME Journal of Engineering for Gas Turbines and Power 110 (1988), 453-461.
30. E.M. Sazhina, S.S. Sazhin, M.R. Heikal, C.J. Marooney, "The Shell autoignition model: applications to gasoline and diesel fuels", Fuel 78 (1999), 389-401.
31. J. Warnatz, U. Maas, R.W. Dibble, "Combustion", Fourth Edition, Springer (2006).
32. P.Q. Tan, Z.Y. Hu, K.Y. Deng, J.X. Lu, D.M. Lou, G. Wan, "Particulate matter emission modelling based on soot and SOF from direct injection diesel engines", Energy Conversion and Management 48 (2007), 510–518.
33. G. D’Errico, G. Ferrari, A. Onorati, T. Cerri, "Modeling the Pollutant Emissions from a S.I. Engine", SAE Paper 2002-01-0006, 2002.

ABBREVIATIONS

CFD Computational Fluid Dynamics
CO Carbon Monoxide
EGR Exhaust Gas Recirculation
HC Unburned Hydrocarbons
HSDI High Speed Direct Injected
LTO Low Temperature Oxidation
NO Nitric oxide
NO_x Nitric oxides (NO, NO_2)
NSC Nagle and Strickland-Constable

NOMENCLATURE

LATIN SYMBOLS

a	Polynomial coefficient
A	Collision frequency factor
A/F	Air-fuel ratio [-]
c	Calibration constant
C	Constant
d	Diameter [m]
E	Activation energy [J mol^{-1}] or [K]
F	Function
J	Jacobian matrix
k_A	NSC model soot oxidation kinetic rate coefficient (A site)
k_B	NSC model soot oxidation kinetic rate coefficient (B site)
k_b	Backward kinetic rate coefficient
k_f	Forward kinetic rate coefficient
k_T	NSC model surface oxidation kinetic rate coefficient
k_Z	NSC model A-site to B-site kinetic rate coefficient
K	Equilibrium constant
m	Mass [kg]
Mi	Generic species
n	Number of moles [mol]
N	Number of sth
p	Pressure [Pa]
r	Radius [m]
R	Universal gas constant [8.31447 J mol^{-1} K^{-1}]
T	Temperature [K]
V	Volume [m^3]
W	Molecular weight [g mol^{-1}]
X	Concentration [kmol m^{-3}]
x	Molar fraction
y	Mass fraction

GREEK SYMBOLS

α	Order of the chemical reaction
ΔG^0	Gibbs free energy change
Δg^0	Std. molar free energy of formation
Φ	Air-fuel mixture equivalence ratio
ν'	Reactant stoichiometric coefficient
ν''	Product stoichiometric coefficient
ρ	Density
Ψ	Ratio between moles of products and moles of reactants

SUBSCRIPTS

a	air
c	carbon
CO	carbon monoxide
EGR	exhaust gas recirculated
ev	evaporated fuel
f	formation
f	fuel
F	referring to multivariate, array function
HC	Unburned Hydrocarbons
imp	Impinged zone
inj	injector
λ	generic species index
l	liquid fuel
L	lean limit
max	maximum
NO	nitric oxide
o	oxidation
p	partial (referred to pressure)
s	soot
sac	Referring to injector sac volume
st	stoichiometric
switch	separation between low and high temperature ranges
u	Universal

CONTACT INFORMATION

Federico Perini
Dipartimento di Ingegneria Meccanica e Civile, Università degli Studi di Modena e Reggio Emilia
strada Vignolese, 905/B - 41125 Modena, Italy
Phone: +39 059 2056101
email: federico.perini@unimore.it